

Spatial sub-Rayleigh imaging via structured speckle illumination

Liming Li*

*School of Physics and Optoelectronic Engineering,
Shandong University of Technology, Zibo 255049, China*

(Dated: July 31, 2024)

In a lens-assisted imaging scheme with speckle illumination, the spatial resolution can surpass the Rayleigh resolution limit by a factor of $\sqrt{2}$ with second-order auto-correlation of light intensity. In this work, integrated with the nonlinear structured illumination after the speckle sinusoidally modulated, the second-order auto-correlation imaging can surpass the Rayleigh resolution limit by a factor of $2 + \sqrt{2}$. In theory, a higher spatial resolution with the surpassing factor $N + \sqrt{N}$ is available by the N -order auto-correlation measurement. Our imaging scheme combined two super-resolution technologies not only enhances the spatial resolution of the lens-assisted imaging, but also promotes the practicality of the intensity correlation imaging.

I. INTRODUCTION

Due to the wave property of light, the image of a point is a spot in a lens-assisted imaging system [1]. With the incoherent illumination, the correspondence of point-to-spot leads to a limited spatial resolution, known as the Rayleigh resolution limit $\Delta\rho_R = 0.61\lambda/\text{NA}$ [2], where λ is the wavelength of light and NA is the numerical aperture of imaging system [3]. In order to improve the spatial resolution with limited NA, some well-designed intelligent schemes have been invented in the field of optical microscopic imaging [4–7]. In 1999, Heintzmann and Cremer proposed that the high frequency information of text object less than twice the cut-off frequency lies inside the support of optical transfer function (OTF) by the aid of the illumination with a laterally modulated light[8]. In the following year Gustafsson proposed the classical two-dimensional structured illumination microscopy (2D-SIM)[9, 10] on the basis of Heintzmann's theory. After projecting sequentially three phase shifted sinusoidally fringes and collecting parallel raw images, people can separate those superposed frequency components by solving a group of linear equations[9, 11]. In theory, the resolution of 2D-SIM can surpass the Rayleigh resolution limit by a factor of 2. What's more, to acquire higher spatial resolution, Heintzmann proposed a non-linear SIM scheme[12], which was named the saturated structured illumination microscopy (SSIM). Later, some works demonstrated the super-resolution potential of SSIM[13, 14].

From the multi-photon interference point of view, some sub-Rayleigh imaging schemes are developed via measurement the high-order correlation of light, such as the N -photon detection [15–17] and the optical centroid measurements [18–20]. Due to weak mechanical structure and expensive detection equipment, the sub-Rayleigh imaging with quantum source is challenge to researchers in the experimental study. To avoid these obstacles,

classical light were employed to acquire spatial high frequency information of text object via intensity correlated measurement [21–27]. In fact, people need to find novel modulation schemes [21–23] or measure the auto-correlation of light intensity [24–27]. For example, some imaging schemes using dynamic complex amplitude modulation can reach the standard quantum limit [21] and the Heisenberg limit [22, 23]. Interestingly, there is a quite simple scheme to achieve sub-Rayleigh image. If the text object is illuminated with dynamic speckle, the resolution by the measurement with N -order auto-correlation of light can surpass the Rayleigh resolution limit by a factor of \sqrt{N} [24–28].

In this work, we theoretically analyzed and numerical experimentally demonstrated a lens-assisted second-order sinusoidally structured speckle illumination microscopy (SSSIM) scheme, whose spatial resolution can surpass the Rayleigh resolution limit by a factor of $2 + \sqrt{2}$. What's more, the surpassing factor of SSSIM scheme is $N + \sqrt{N}$ through N -order correlation of light.

II. THEORY

Figure 1 depicts the SSSIM experimental setup, which includes a $2f - 2f$ imaging system and a controllable dynamic speckle illumination system. A continuous-wave $\lambda = 632.8$ nm single-mode laser beam was expanded and collimated by a beam expander (BE), and was then reflected by a 50:50 non-polarized beam splitter (BS1) onto a phase-only reflective spatial light modulator (SLM1, an element pixel size of $24.6 \times 24.6 \mu\text{m}^2$ and a total pixels 512×512). The reflected beam from the SLM1 transmitted through the BS1 again and was then refracted by a lens (L1) with a focal length $f_1 = 80$ cm. Here, a amplitude-only reflective SLM2 (an element pixel size of $20 \times 20 \mu\text{m}^2$ and a total pixels 512×512) was put on the rear focal plane of L1. Therefore, the dynamic speckle illumination can be realize on the plane of SLM2 while the random phase pattern was encoded onto the wavefront of light by reflected from the SLM1 [29–31]. In addition, it's easy to control the size of speckle particle by

* liliming@sdut.edu.cn

decides the frequency shift. Comparing with $\widetilde{T}^4(k)$ the zero-fold frequency shift domain (FSD₀) in Eq. (6), $\widetilde{T}^4(k - \vec{p}_\varphi \cdot \vec{\rho}_o)$, $\widetilde{T}^4(k + \vec{p}_\varphi \cdot \vec{\rho}_o)$, $\widetilde{T}^4(k - 2\vec{p}_\varphi \cdot \vec{\rho}_o)$ and

$\widetilde{T}^4(k + 2\vec{p}_\varphi \cdot \vec{\rho}_o)$ are FSD₁, FSD₋₁, FSD₂ and FSD₋₂, respectively. Although superposed together, those five FSDs can be separated by the linear equation:

$$\begin{bmatrix} \widetilde{T}^4(k) \widetilde{H}^2(k) \\ \widetilde{T}^4(k - \vec{p}_\varphi \cdot \vec{\rho}_o) \widetilde{H}^2(k) \\ \widetilde{T}^4(k + \vec{p}_\varphi \cdot \vec{\rho}_o) \widetilde{H}^2(k) \\ \widetilde{T}^4(k - 2\vec{p}_\varphi \cdot \vec{\rho}_o) \widetilde{H}^2(k) \\ \widetilde{T}^4(k + 2\vec{p}_\varphi \cdot \vec{\rho}_o) \widetilde{H}^2(k) \end{bmatrix} = \begin{bmatrix} \frac{3}{2} & -e^{i\phi_1} & -e^{-i\phi_1} & \frac{1}{4}e^{2i\phi_1} & \frac{1}{4}e^{-2i\phi_1} \\ \frac{3}{2} & -e^{i\phi_2} & -e^{-i\phi_2} & \frac{1}{4}e^{2i\phi_2} & \frac{1}{4}e^{-2i\phi_2} \\ \frac{3}{2} & -e^{i\phi_3} & -e^{-i\phi_3} & \frac{1}{4}e^{2i\phi_3} & \frac{1}{4}e^{-2i\phi_3} \\ \frac{3}{2} & -e^{i\phi_4} & -e^{-i\phi_4} & \frac{1}{4}e^{2i\phi_4} & \frac{1}{4}e^{-2i\phi_4} \\ \frac{3}{2} & -e^{i\phi_5} & -e^{-i\phi_5} & \frac{1}{4}e^{2i\phi_5} & \frac{1}{4}e^{-2i\phi_5} \end{bmatrix}^{-1} \begin{bmatrix} \Delta G_{\varphi, \phi_1}^{(2)}(k) \\ \Delta G_{\varphi, \phi_2}^{(2)}(k) \\ \Delta G_{\varphi, \phi_3}^{(2)}(k) \\ \Delta G_{\varphi, \phi_4}^{(2)}(k) \\ \Delta G_{\varphi, \phi_5}^{(2)}(k) \end{bmatrix}, \quad (8)$$

where $[M]^{-1}$ means the inverse matrix of M . As we can see, five independent measurements with different ϕ can give those five FSDs in the orientation of φ . With the frequency expansion at four orientations, the circle of OTF support of second-order SSSIM is $(2 + \sqrt{2})p$ as shown in Fig. 2(d). Considering the similarity of frequency operations (Shift, Merge and Inverse Fourier transformation) with 2D-SIM, we will not elaborate on it here. Please refer to the 2D-SIM [11]. In the following section, we will verify the spatial high-resolution of the SSSIM scheme.

III. NUMERICAL EXPERIMENT

In order to test the spatial resolution of SSSIM, we perform the follow-up numerical experiment. To create the dynamic speckle illumination system, the phase structure $e^{i\theta(\rho_s, t)}$ were loaded on the SLM1, where the phasor $\theta(\rho_s, t) \in [0, 2\pi)$ is completely random in the spatial ρ_s and the time t distribution. The average size l_c of speckle particle (i.e. the transverse coherence length) on the object plane is $\lambda f_1 / \Delta L_1 = 85 \mu\text{m}$, where the diameter of iris1 ΔL_1 is 6 mm. What's more, the Rayleigh-resolution limit $\Delta\rho_R$ of the $2f_2 - 2f_2$ imaging system is 1 mm. Therefore, the average size of speckle particle meets the requirement of auto-correlation imaging scheme.

Figure 3 gives the numerical experiment with a 0-1 binary text object '*' and a natural grayscale text object 'Cameraman'. The number of total frame is 10000 for the second-order auto-correlation imaging and those raw images in the SSSIM scheme. Figures 3 (a1, a3) show those test objects, which are 512×512 pixels. The imaging results of first-order intensity imaging and second-order auto-correlation imaging are shown in Figs. 3(b1, b3) and Figs. 3(c1, c3), respectively. Although the circle of OTF support of auto-correlation imaging scheme is larger than that of the first-order intensity imaging, the improvement of spatial resolution is inapparent. However, as the frequency detection domain further expanded, those imaging results will present more details. The imaging results of 2D-SIM and SSSIM are shown in Figs. 3(d1, d3) and

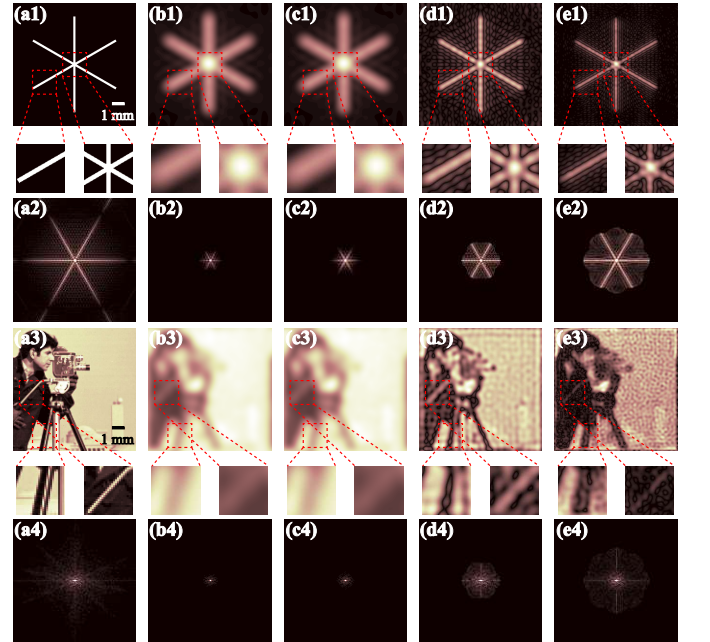


FIG. 3. Test objects: (a1), (a3); the first-order intensity imaging: (b1), (b3); the second-order auto-correlation imaging: (c1), (c3); 2D-SIM: (d1), (d3); SSSIM: (e1), (e3); (a2-e2, a4-e4) Fourier domain of images in (a1-e1, a3-e3), respectively. Those insets show the enlarged details of images.

Figs. 3(e1, e3), respectively. Herein the 2D-SIM scheme, the orientation and the phase of sinusoidal illumination pattern satisfy $\varphi \in [0, \pi/3, 2\pi/3]$ and $\phi \in [0, 2\pi/3, 4\pi/3]$, respectively. As we can see, those imaging results with 2D-SIM scheme and SSSIM scheme show significant improvement on the spatial resolution whether 0-1 binary object or natural grayscale object. From those details of images shown in the insets, we can further find that the resolution of SSSIM is higher than the 2D-SIM. Figures 3(a2-e2, a4-e4) present the Fourier domain of images in Figs.3 (a1-e1, a3-e3), respectively. As we can see, those Fourier domains in Figs. 3(b2-e2, b4-e4) are similar with

the corresponding OTF support as shown in Fig. 2.

The fidelity of imaging result can be estimated by calculating the peak signal-to-noise ratio (PSNR):

$$\text{PSNR} = 10 \log_{10} [(2^{\text{BIT}} - 1)^2 / \text{MSE}], \quad (9)$$

where $\text{BIT} = 8$ is the bit depth of images and MSE is the mean-square error of the imaging result with respect to the test object. Here, MSE is defined as:

$$\text{MSE} = \frac{1}{\tau^2} \sum_{n_1=1}^{\tau} \sum_{n_2=1}^{\tau} [I(n_1, n_2) - T(n_1, n_2)]^2, \quad (10)$$

where $\tau = 512$ is the total number of pixels in single dimension. The imaging result $I(n_1, n_2)$ and the test object $T(n_1, n_2)$ are digitized to $0 \sim 255$. It can be seen that the higher the quality of the result, the greater the PSNR. According to numerical results, PSNR of Figs. 3(b1-e1) with the 0-1 binary object are 14.74 dB, 15.20 dB, 17.82 dB and 16.50 dB, respectively. What's more, PSNR of Figs. 3(b3-e3) with the grayscale object are 5.47 dB, 5.52 dB, 16.78 dB and 16.39 dB, respectively. It can be seen that the quality of image results has been optimized through the 2D-SIM scheme and the SSSIM scheme. Although the SSSIM scheme acquires more frequency information and displays more object details, the image quality is slightly lower than the 2D-SIM scheme. Considering that those imaging results with the SSSIM scheme originated from the frequency merge by 25 FSDs and the number is 9 for 2D-SIM, the frequency merge leads to substantial ringing effect so that a serious loss in imaging quality. If denoising and filtering techniques of 2D-SIM [33–36] can be appropriately introduced, the imaging quality will be improved and the imaging results can show more details of text object.

IV. DISCUSSION

In theory, the spatial resolution of SSSIM can be further improved through high-order correlation of light. The N -order fluctuation auto-correlation function on the image plane with speckle illumination sinusoidally modulated can be expressed as:

$$\Delta G_{\varphi, \phi}^{(N)}(\vec{\rho}_i) = [SI_{\varphi, \phi}^N(\vec{\rho}_o) T^{2N}(\vec{\rho}_o)] \otimes H^N(\vec{\rho}_i - \vec{\rho}_o), \quad (11)$$

where the modulation term $SI_{\varphi, \phi}^N(\vec{\rho}_o)$ desides FSD of SS-SIM. Here, those Fourier transform of modulation terms with $N = 3$ and $N = 4$ are expressed as:

$$\begin{aligned} \widetilde{SI_{\varphi, \phi}^3}(k) = & \frac{5}{2} \delta(k) \\ & - \frac{15}{8} e^{i\phi} \delta(k - \vec{p}_{\varphi} \cdot \vec{\rho}_o) - \frac{15}{8} e^{-i\phi} \delta(k + \vec{p}_{\varphi} \cdot \vec{\rho}_o) \\ & + \frac{3}{4} e^{2i\phi} \delta(k - 2\vec{p}_{\varphi} \cdot \vec{\rho}_o) + \frac{3}{4} e^{-2i\phi} \delta(k + 2\vec{p}_{\varphi} \cdot \vec{\rho}_o) \\ & - \frac{1}{8} e^{3i\phi} \delta(k - 3\vec{p}_{\varphi} \cdot \vec{\rho}_o) - \frac{1}{8} e^{-3i\phi} \delta(k + 3\vec{p}_{\varphi} \cdot \vec{\rho}_o) \end{aligned} \quad (12)$$

and

$$\begin{aligned} \widetilde{SI_{\varphi, \phi}^4}(k) = & \frac{35}{8} \delta(k) \\ & - \frac{7}{2} e^{i\phi} \delta(k - \vec{p}_{\varphi} \cdot \vec{\rho}_o) - \frac{7}{2} e^{-i\phi} \delta(k + \vec{p}_{\varphi} \cdot \vec{\rho}_o) \\ & + \frac{7}{4} e^{2i\phi} \delta(k - 2\vec{p}_{\varphi} \cdot \vec{\rho}_o) + \frac{7}{4} e^{-2i\phi} \delta(k + 2\vec{p}_{\varphi} \cdot \vec{\rho}_o) \\ & - \frac{1}{2} e^{3i\phi} \delta(k - 3\vec{p}_{\varphi} \cdot \vec{\rho}_o) - \frac{1}{2} e^{-3i\phi} \delta(k + 3\vec{p}_{\varphi} \cdot \vec{\rho}_o) \\ & + \frac{1}{16} e^{4i\phi} \delta(k - 4\vec{p}_{\varphi} \cdot \vec{\rho}_o) + \frac{1}{16} e^{-4i\phi} \delta(k + 4\vec{p}_{\varphi} \cdot \vec{\rho}_o), \end{aligned} \quad (13)$$

respectively. Therefore, it is easy to find that the circle of OTF support with N -order SSSIM scheme is $(N + \sqrt{N})p$.

TABLE 1. The proportion in percentage of each PSD in SS-SIM scheme at the case of $N = 2, 3, 4$.

% \ FSD	-4	-3	-2	-1	0	1	2	3	4
order									
N=2	0	0	6.25	25	37.5	25	6.26	0	0
N=3	0	1.56	9.38	23.44	31.25	23.44	9.38	1.56	0
N=4	0.39	3.13	10.94	21.88	27.34	21.88	10.94	3.13	0.39

As we can see, different order N in SSSIM scheme leads to changes in the proportion of various FSDs. Table 1 shows the proportion in percentage of each PSD in the case of $N = 2, 3, 4$. Here, the total percentage is obtained by summing the absolute values of the weights of each PSDs in the Fourier transform of modulation terms. It is worth noting that the proportion of FSD_N in the N -order SSSIM scheme is small, such as the percentage of FSD_4 is only 0.39%. Therefore, a low sampling and high image quality algorithm is key for the auto-correlation of light intensity.

V. CONCLUSION

In conclusion, we proposed theoretically and demonstrated numerical experimentally the sub-Rayleigh second-order SSSIM scheme. The spatial resolution can surpass the Rayleigh resolution limit by a factor of $2 + \sqrt{2}$. The SSSIM scheme is effective whether for 0-1 binary object or natural grayscale object. What's more, the spatial resolution with N -order SSSIM scheme can surpass the Rayleigh resolution limit by a factor of $N + \sqrt{N}$. However, the suppression of noise plays a key role to ensure a high signal-to-noise ratio for the FSD_N signal.

ACKNOWLEDGEMENTS

Liming Li thanks Qiulan Liu for helpful discussions. This work is financially supported by the National Natural Science Foundation of China (NSFC) (62105188).

-
- [1] M. Born and E. Wolf, *Principles of Optics* (Cambridge University Press, 1999).
 - [2] F. R. S. Lord Rayleigh, "Investigations in optics, with special reference to the spectroscope," *Phil. Mag.* **8**, 261 (1879).
 - [3] J. W. Goodman, *Introduction to Fourier optics* (Roberts and Company publishers, 2005).
 - [4] S. W. Hell and J. Wichmann, "Breaking the diffraction resolution limit by stimulated emission: stimulated-emission-depletion fluorescence microscopy," *Opt. Lett.* **19**, 780 (1994).
 - [5] E. Betzig, G. H. Patterson, R. Sougrat, *et al.*, "Imaging intracellular fluorescent proteins at nanometer resolution," *Science* **313**, 1642 (2006).
 - [6] M. J. Rust, M. Bates, and X. Zhuang, "Sub-diffraction-limit imaging by stochastic optical reconstruction microscopy (STORM)," *Nat. Methods* **3**, 793 (2006).
 - [7] B. Huang, W. Wang, M. Bates, *et al.*, "Three-dimensional super-resolution imaging by stochastic optical reconstruction microscopy," *Science* **319**, 810 (2008).
 - [8] R. Heintzmann and C. G. Cremer, "Laterally modulated excitation microscopy: improvement of resolution by using a diffraction grating," *Proc. SPIE* **3568**, 185 (1999).
 - [9] M. G. Gustafsson, D. A. Agard, and J. W. Sedat, "Doubling the lateral resolution of wide-field fluorescence microscopy using structured illumination," *Proc. SPIE* **3919**, 141 (2000).
 - [10] M. G. Gustafsson, "Surpassing the lateral resolution limit by a factor of two using structured illumination microscopy," *J. Microsc.* **198**, 82 (2000).
 - [11] A. Lal, C. Shan, and P. Xi, "Structured Illumination Microscopy Image Reconstruction Algorithm," *IEEE J. Sel. Top. Quantum Electronics* **22**, 6803414 (2016).
 - [12] R. Heintzmann, T. M. Jovin, and C. Cremer, "Saturated patterned excitation microscopy—a concept for optical resolution improvement," *JOSA A* **19**, 1599 (2002).
 - [13] M. G. Gustafsson, "Nonlinear structured-illumination microscopy: wide-field fluorescence imaging with theoretically unlimited resolution," *Proc. Natl. Acad. Sci. United States Am.* **102**, 13081 (2005).
 - [14] E. H. Rego, L. Shao, J. J. Macklin, *et al.*, "Nonlinear structured-illumination microscopy with a photoswitchable protein reveals cellular structures at 50-nm resolution," *Proc. Natl. Acad. Sci. United States Am.* **109**, 135 (2012).
 - [15] V. Giovannetti, S. Lloyd, L. Maccone, *et al.*, "Sub-Rayleigh-diffraction-bound quantum imaging," *Phys. Rev. A* **79**, 013827 (2009).
 - [16] F. Guerrieri, L. Maccone, F. N. C. Wong, *et al.*, "Sub-Rayleigh Imaging via N-Photon Detection," *Phys. Rev. Lett.* **105**, 163602 (2010).
 - [17] D.-Q. Xu, X.-B. Song, H.-G. Li, *et al.*, "Experimental observation of sub-Rayleigh quantum imaging with a two-photon entangled source," *Appl. Phys. Lett.* **106**, 171104 (2015).
 - [18] M. Unternährer, B. Bessire, L. Gasparini, *et al.*, "Super-resolution quantum imaging at the Heisenberg limit," *Optica* **5**, 1150 (2018).
 - [19] M. Tsang, "Quantum imaging beyond the diffraction limit by optical centroid measurements," *Phys. Rev. Lett.* **102**, 253601 (2009).
 - [20] E. Toninelli, P.-A. Moreau, and T. Gregory, "Resolution-enhanced quantum imaging by centroid estimation of biphotons," *Optica* **6**, 347 (2019).
 - [21] E. Zhang, H. Lin, W. Liu, *et al.*, "Sub-Rayleigh-diffraction imaging via modulating classical light," *Opt. Express* **23**, 33506 (2015).
 - [22] P. Hong and G. Zhang, "Heisenberg-resolution imaging through a phase-controlled screen," *Opt. Express* **25**, 22789 (2017).
 - [23] L. Li, P. Hong, and G. Zhang, "Experimental realization of Heisenberg-limit resolution imaging through a phase-controlled screen with classical light," *Opt. Express* **26**, 18950 (2018).
 - [24] T. Dertinger, R. Colyer, G. Iyer, *et al.*, "Fast, background-free, 3D super-resolution optical fluctuation imaging (SOFI)," *Proc. Natl. Acad. Sci. United States Am.* **106**, 22287 (2009).
 - [25] J.-E. Oh, Y.-W. Cho, G. Scarcelli, *et al.*, "Sub-Rayleigh imaging via speckle illumination," *Opt. Lett.* **38**, 682 (2013).
 - [26] Y. Wang, F. Wang, R. Liu, *et al.*, "Spatial sub-Rayleigh imaging analysis via speckle laser illumination," *Opt. Lett.* **40**, 5323 (2015).
 - [27] L.-Y. Dou, D.-Z. Cao, L. Gao, *et al.*, "Sub-Rayleigh dark-field imaging via speckle illumination," *Opt. Lett.* **48**, 1347 (2023).
 - [28] F. Li, C. Altuzarra, T. Li, *et al.*, "Beyond sub-Rayleigh imaging via high order correlation of speckle illumination," *J. Opt.* **21**, 115604 (2019).
 - [29] L. Li, P. Hong, and G. Zhang, *et al.*, "Transverse revival and fractional revival of the Hanbury Brown and Twiss bunching effect with discrete chaotic light," *Phys. Rev. A* **99**, 023848 (2019).
 - [30] L. Li, B. Wang, S. Li, *et al.*, "Eigenmode high-visibility imaging in the far-field ghost imaging system with discrete chaotic light," *Phys. Lett. A* **420**, 127749 (2021).
 - [31] X. Wu, Y. Zhao, and L. Li, "High-visibility ghost imaging with phase-controlled discrete classical light sources," *Chin. Phys. B* **33**, 074202 (2024).
 - [32] J. W. Goodman, *Introduction to Fourier Optics* (Roberts and Company Publishers, 1995).
 - [33] M. G.L. Gustafsson, L. Shao, P. M. Carlton, *et al.*, "Three-dimensional resolution doubling in wide-field fluorescence microscopy by structured illumination," *Biophys. J.* **94** P4957 (2008).
 - [34] M. Müller, V. Mönkemöller, S. Hennig, *et al.*, "Open-source image reconstruction of super-resolution structured illumination microscopy data in ImageJ," *Nat. Commun.* **7** 10980 (2016).
 - [35] G. Wen, S. Li, L. Wang, *et al.*, "High-fidelity structured illumination microscopy by point-spreadfunction engineering," *Light Sci. Appl.* **10** 70 (2021).
 - [36] C. S. Smith, J. A. Slotman, L. Schermelleh, *et al.*, "Structured illumination microscopy with noisecontrolled image reconstructions," *Nat. Methods*, **18** 821 (2021).